

DOI: 10.1002/cctc.201300813

Nickel–Gallium Intermetallic Nanocrystal Catalysts in the Semihydrogenation of Phenylacetylene

Changming Li, Yudi Chen, Shitong Zhang, Junyao Zhou, Fei Wang, Shan He, Min Wei,*
David G. Evans, and Xue Duan^[a]

The chemoselective hydrogenation of alkyne is of great importance in the chemical industry, in which intermetallic compounds (IMCs) have attracted extensive interest as efficient catalysts. Herein, we demonstrate the preparation of several supported Ni–Ga IMCs (Ni₃Ga, Ni₅Ga₃, and NiGa) via a facile in situ reduction of layered double hydroxide (LDH) precursors, which demonstrate significantly improved catalytic activity and selectivity for the selective hydrogenation of phenylacetylene to styrene. The composition and particle size of Ni–Ga IMCs can be tuned by adjusting the Ni/Ga ratio or reduction temperature during the topotactic transformation process of LDHs, and

the best catalytic behavior can be obtained over the Ni₃Ga IMC with a styrene yield of 87.7% (particle size = 7.2 nm at 40 °C and 0.3 MPa), which is better than that of most of the reported Ni catalysts. The X-ray absorption fine-structure characterization and DFT calculations reveal the electron transfer from Ga to Ni and active-site isolation by Ga in Ni–Ga IMCs, which account for the excellent hydrogenation selectivity. The significantly improved catalytic performance makes Ni–Ga IMC catalysts promising candidates for the selective hydrogenation of alkyne.

Introduction

Phenylacetylene removal in styrene feedstocks through semihydrogenation is an important industrial process owing to its serious poisoning effect on styrene polymerization catalysts, and the selective hydrogenation of phenylacetylene to styrene has been commonly used.^[1] The main challenge in this process is to develop effective catalysts with satisfactory activity and high selectivity to avoid the complete hydrogenation of phenylacetylene to ethylbenzene. Palladium-based catalysts have received considerable attention owing to their good hydrogenation selectivity toward alkene (e.g., in the dispersed colloids^[2] and supported systems^[3]). Although great progress has been made, the limited resource and high cost of noble Pd limit their practical applications in the industry. Therefore, the design and fabrication of efficient and cost-effective substitutes are desirable and remain a challenging goal.

Intermetallic compounds (IMCs) with their unique electronic structures and geometries^[4] have attracted extensive research interest in catalysis, for instance, hydrogenation of unsaturated aldehydes on RuTi or NiSn IMCs,^[5] methanol synthesis and methanol steam reforming on PdGa and PdZn IMCs,^[6] and fuel electrocatalytic oxidation over Pt₃Ti or PtPb IMCs.^[7] Armbrüster et al. recently developed a series of IMCs (e.g., PdGa IMC^[8] and

Al₁₃Fe₄ IMC^[9]) as effective catalysts for the selective hydrogenation of acetylene to ethylene, the improved catalytic selectivity of which is attributed to the combination of the electronic structure and site-isolation effect. Although considerable effort has been devoted to the preparation of IMCs by using chemical colloidal methods,^[10] and their desirable catalytic behavior has been demonstrated, they still inevitably require expensive noble metals and costly and toxic organic reagents, damaged activity by capping reagents, or serious self-agglomeration in the reaction process. Therefore, it is highly essential to develop facile and green strategies for the synthesis of IMCs serving as efficient catalysts.

Layered double hydroxides (LDHs) are a class of naturally occurring and synthetic materials generally expressed by the formula [M_{1–x}²⁺M_x³⁺(OH)₂](A^{n–})_{x/n}·mH₂O, in which M²⁺ and M³⁺ cations disperse in an ordered and uniform manner in brucite-like layers.^[11] Considerable interest has been focused on LDH materials as heterogeneous catalysts on the basis of their versatility in chemical composition and structural architecture.^[12] A topotactic transformation of LDH materials to uniformly dispersed metal nanoparticles (NPs) supported on metal oxide matrix occurs under reducing conditions.^[13] Inspired by the structural merits of LDH materials, we explored the idea of incorporating highly active but lowly selective Ni and inactive but more electropositive Ga species into the LDH precursors followed by a reduction process to fabricate non-noble Ni–Ga IMC (e.g., Ni₃Ga, Ni₅Ga₃, and NiGa) catalysts for the selective hydrogenation of phenylacetylene. This strategy would possess the following desirable features: 1) the atomic scale interspersion of Ni and Ga species in the LDH precursors would facilitate the formation of highly dispersed Ni–Ga IMCs under mod-

[a] Dr. C. Li, Y. Chen, Dr. S. Zhang, J. Zhou, Dr. F. Wang, Dr. S. He, Prof. M. Wei, Prof. D. G. Evans, Prof. X. Duan
State Key Laboratory of Chemical Resource Engineering
Beijing University of Chemical Technology
Beijing 100029 (P.R. China)
Fax: (+86) 10-64425385
E-mail: weimin@mail.buct.edu.cn

 Supporting information for this article is available on the WWW under <http://dx.doi.org/10.1002/cctc.201300813>.

erate reduction conditions, and 2) the catalytic performance of Ni–Ga IMCs can be tuned by changing the Ni/Ga ratio in LDH precursors.

Herein, we report the fabrication of several supported Ni–Ga IMCs (Ni_3Ga , Ni_5Ga_3 , and NiGa) with tunable particle size by using the LDH precursor method and demonstrate their application as efficient catalysts for the selective hydrogenation of phenylacetylene. The composition and particle size of the supported Ni–Ga IMCs can be tuned by changing the Ni/Ga ratio or reduction temperature during the topotactic transformation of LDHs. The X-ray absorption fine-structure (XAFS) characterization demonstrates the relatively low Ni K-edge X-ray absorption near-edge structure (XANES) absorption edge and low coordination number in Ni–Ga IMCs compared with the Ni foil, implying the charge transfer from Ga to Ni and active-site isolation by Ga, which were confirmed by DFT calculations. The resulting materials demonstrate significantly improved catalytic selectivity for the hydrogenation of phenylacetylene to styrene, and the best catalytic behavior was obtained over the Ni_3Ga IMC with a styrene yield of 87.7% (particle size = 7.2 nm at 40 °C and 0.3 MPa), which is better than that of most of the reported Ni catalysts. The remarkably increased hydrogenation selectivity can be attributed to the observed Ni–Ga synergistic effect. Our approach holds significant promise for Ni–Ga IMCs as efficient catalysts for the selective hydrogenation of phenylacetylene.

Results and Discussion

Structure and morphology of $\text{Ni}_x\text{Mg}_y\text{Ga}_z$ LDH precursors

$\text{Ni}_x\text{Mg}_y\text{Ga}_z$ LDH precursors were prepared by using the coprecipitation method. The XRD patterns of $\text{Ni}_x\text{Mg}_y\text{Ga}_z$ LDHs with various Ni/Mg/Ga ratios, all of which can be indexed as a rhombohedral structure with the typical (003), (006), (012), (013), (110), and (113) reflections at $2\theta \approx 11.2$, 22.7, 34.2, 38.5, 59.8, and 61.2° for LDH materials, respectively, are shown in Figure 1. No other crystalline phase was detected, which indicated the high purity of these LDH materials. The small difference in the 2θ reflections among the four LDH precursors is

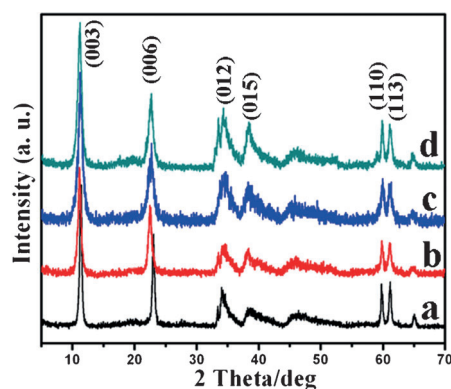


Figure 1. XRD patterns of the as-synthesized $\text{Ni}_x\text{Mg}_y\text{Ga}_z$ LDH precursors with various $x(\text{Ni})/y(\text{Mg})/z(\text{Ga})$ ratios: a) NiMg_3Ga_4 -LDHs, b) NiMg_3Ga -LDHs, c) $\text{Ni}_5\text{Mg}_4\text{Ga}_3$ -LDHs, and d) $\text{Ni}_3\text{Mg}_2\text{Ga}$ -LDHs.

due to their different metal proportion and ionic radius. The initial and the resulting metal ratios of the products determined from inductively coupled plasma atomic emission spectroscopy analysis are summarized in Table S1, which indicates that the metal ratios in these products are similar to those in the feed intake. The SEM images (Figure 2) of $\text{Ni}_x\text{Mg}_y\text{Ga}_z$ LDHs show that all the LDH precursors demonstrate a typical nanoplatelet morphology with a diameter of 30–100 nm, which indicates their proper crystallization.

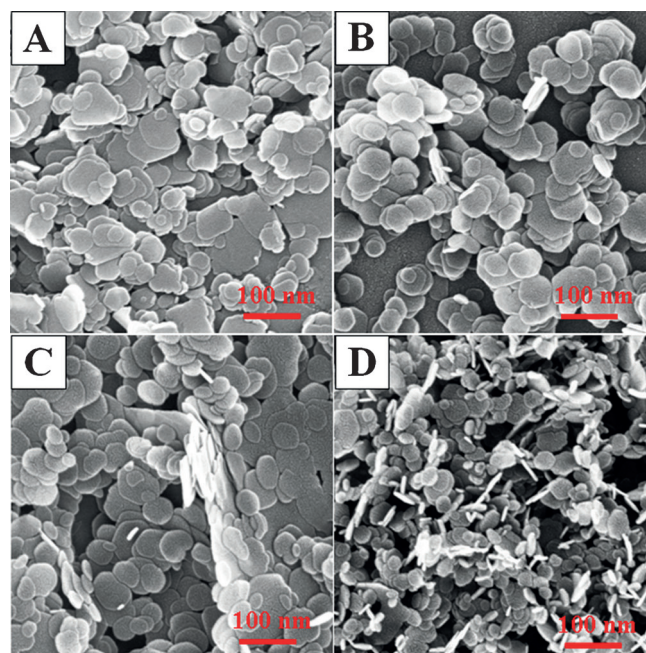


Figure 2. SEM images of the as-synthesized $\text{Ni}_x\text{Mg}_y\text{Ga}_z$ LDH precursors with various $x(\text{Ni})/y(\text{Mg})/z(\text{Ga})$ ratios: A) NiMg_3Ga_4 -LDHs, B) NiMg_3Ga -LDHs, C) $\text{Ni}_5\text{Mg}_4\text{Ga}_3$ -LDHs, and D) $\text{Ni}_3\text{Mg}_2\text{Ga}$ -LDHs.

Topotactic transformation from LDH materials to supported Ni–Ga IMCs

To study the topotactic transformation of $\text{Ni}_x\text{Mg}_y\text{Ga}_z$ LDH materials to Ni–Ga IMCs, the temperature-programmed reduction by H_2 (H_2 -TPR) measurements was performed with Ni_2Al LDHs as reference samples (Figure 3). The peak below 400 °C is assigned to the reduction of Ni species in $\text{Ni}_x\text{Mg}_y\text{Ga}_z$ LDHs (Figure 3b–e) compared with the reduction peak at 361 °C for Ni_2Al -LDHs (Figure 3a). The peak above 400 °C can be assigned to the reduction of Ga species owing to the high temperature required for reduction.^[14] Three main peaks were observed in the range 400–900 °C for the four $\text{Ni}_x\text{Mg}_y\text{Ga}_z$ LDH samples (Figure 3b–e), which indicated the gradual reduction of Ga species ($\text{Ga}^{3+}/\text{Ga}^{2+}/\text{Ga}^0$) with the increase in reduction temperature.^[14] With the increase in Ni/Ga ratio in $\text{Ni}_x\text{Mg}_y\text{Ga}_z$ LDHs (from Figure 3b to Figure 3e), the reduction temperature of Ga decreases significantly, indicating a Ni-promoted reduction of Ga species to produce Ni–Ga IMCs, which has also been reported in other bimetal reduction processes (e.g., Pa–Ga system^[6a]). The observed Ni-promoted reduction of Ga species may offer an

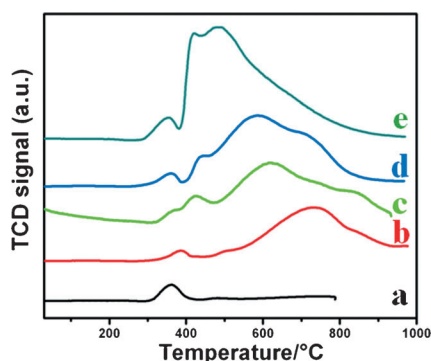


Figure 3. H₂-TPR profiles of a) Ni₂Al-LDHs, b) NiMg₃Ga₄-LDHs, c) NiMg₃Ga-LDHs, d) Ni₃Mg₄Ga₃-LDHs, and e) Ni₃Mg₂Ga-LDHs. TCD = thermal conductivity detector.

opportunity for the controlled synthesis of Ni–Ga IMCs with tunable composition.

We first performed the reduction of Ni_xMg_yGa_z LDHs at 500 °C for 4 h (labeled as Ni_xMg_yGa_z-500) to obtain Ni–Ga IMCs; the XRD patterns of the resulting products are shown in Figure 4. The MgO phase at $2\theta \approx 36.7, 43.1,$ and 62.3° is ob-

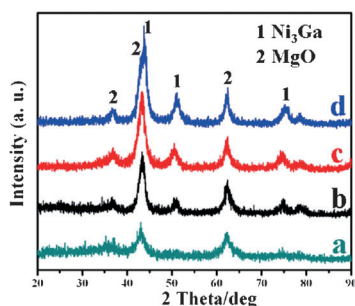


Figure 4. XRD patterns of the as-synthesized Ni–Ga IMCs derived from the in situ reduction of Ni_xMg_yGa_z LDH precursors at 500 °C: a) NiMg₃Ga₄-500, b) NiMg₃Ga-500, c) Ni₃Mg₄Ga₃-500, and d) Ni₃Mg₂Ga-500.

served for all the four samples, which is derived from the calcination of a Mg source in the LDH precursors. The 2θ at $\approx 43.88, 50.94,$ and 75.25° can be indexed to a Ni₃Ga IMC phase (PDF 65-0141). For the NiMg₃Ga₄-500 sample, a weak reflection intensity of Ni₃Ga was observed (Figure 4a). With the increase in Ni/Ga ratio in Ni_xMg_yGa_z LDHs, the intensity of Ni₃Ga IMC increases in the following order: NiMg₃Ga₄-500 < NiMg₃Ga-500 < Ni₃Mg₄Ga₃-500 < Ni₃Mg₂Ga-500 (Figure 4a–d). This result suggests that a higher Ni/Ga ratio facilitates the reduction of Ga and the formation of Ni₃Ga species with larger crystal size, which is responsible for the better defined XRD pattern. This observation will be further demonstrated by TEM images.

The SEM images in Figure S1 reveal that the morphology of the reduced products Ni_xMg_yGa_z-500 inherits the original plate-like morphology of LDH precursors. The detailed structural feature of the obtained Ni₃Ga IMC was further revealed by TEM and high-resolution TEM characterizations (Figure 5). Notably, only Ni₃Ga phase was obtained according to the Ni₃Ga (111)

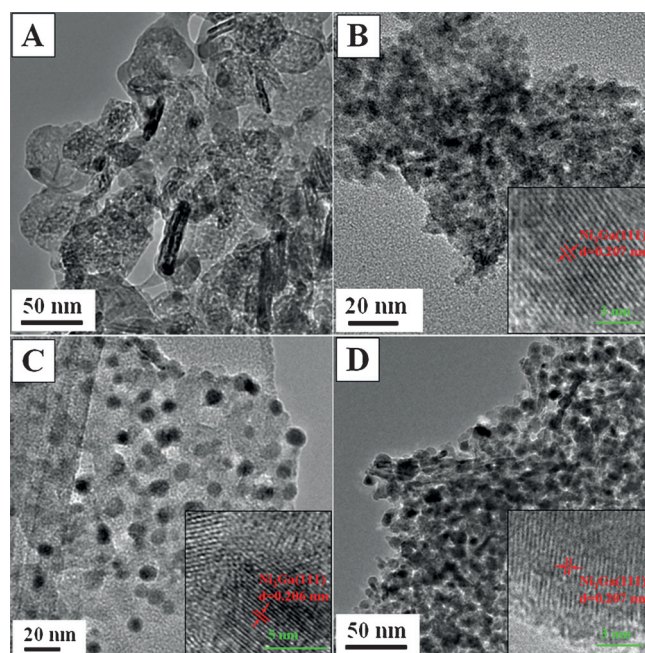


Figure 5. TEM images of the as-synthesized Ni₃Ga NPs derived from the in situ reduction of Ni_xMg_yGa_z LDH precursors at 500 °C: A) NiMg₃Ga₄-500, B) NiMg₃Ga-500, C) Ni₃Mg₄Ga₃-500, and D) Ni₃Mg₂Ga-500. The insets show the high-resolution TEM lattice fringe images assigned to the Ni₃Ga IMC phase.

lattice spacing of 0.207 nm for all the four samples. Only few Ni₃Ga NPs were found for the NiMg₃Ga₄-500 sample (Figure 5a) owing to the low reduction degree of Ga species. With the increase in Ni/Ga ratio, both the particle size and the density increase significantly, which can be attributed to the improvement in the reduction degree of Ga species. The size distribution and mean particle size were also statistically analyzed by measurement over 100 particles (Figure S2). The average size of Ni₃Ga NPs was calculated to be 4.8, 7.2, and 10.9 nm for NiMg₃Ga-500, Ni₃Mg₄Ga₃-500, and Ni₃Mg₂Ga-500, respectively. In brief, Ni₃Ga IMCs with various particle sizes and loading densities can be obtained by controlling the reduction degree of Ga species via different Ni/Ga ratios in Ni_xMg_yGa_z LDH precursors.

In the phase diagram of the Ni–Ga system,^[15] a series of Ni–Ga IMCs can be formed, such as Ni₅Ga₃, NiGa, and NiGa₄. According to the H₂-TPR results (Figure 3), more Ga species in LDHs would be reduced at a high temperature, which may result in other Ni–Ga IMCs with large Ni/Ga ratios. To obtain Ni_xGa_y IMCs with various Ni/Ga ratios, we further explored the calcination of LDH precursors at a higher temperature (700 °C; labeled as Ni_xMg_yGa_z-700) in H₂ atmosphere; the XRD patterns of the resulting products are shown in Figure 6. For the NiMg₃Ga₄-700 sample, a series of reflections at $2\theta \approx 44.3, 64.6,$ and 81.6° are observed (Figure 6a), which correspond to the formation of NiGa IMC (PDF 65-6413). The NiMg₃Ga-700 sample demonstrates 2θ at $\approx 43.3, 48.3, 54.6,$ and 86.8° , which can be assigned to the typical (221), (002), (040), and (223) reflections of a Ni₅Ga₃ IMC (Figure 6b). In the cases of Ni₃Mg₄Ga₃-700 and Ni₃Mg₂Ga-700 (Figure 6c and d), (111), (200), and

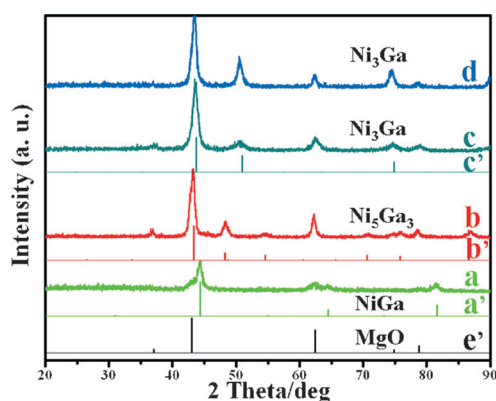


Figure 6. XRD patterns of the as-synthesized Ni-Ga IMCs derived from the in situ reduction of $Ni_xMg_yGa_z$ LDH precursors at 700 °C: a) $NiMg_3Ga_4$ -700, b) $NiMg_3Ga_4$ -700, c) $Ni_5Mg_4Ga_3$ -700, and d) $Ni_3Mg_2Ga_1$ -700. The XRD standard patterns for the corresponding Ni-Ga IMCs and MgO phase are shown in a') NiGa IMC (PDF 65-6413), b') Ni_5Ga_3 IMC (PDF 43-1376), c') Ni_3Ga IMC (PDF 65-0141), and e') MgO (PDF 65-0476).

(220) reflections of a Ni_3Ga phase are obtained, which indicate that both the calcination products are Ni_3Ga IMCs. As a result, two new Ni-Ga IMCs (NiGa and Ni_5Ga_3) were obtained at an increased reduction temperature.

After the reduction at 700 °C, the resulting $Ni_xMg_yGa_z$ -700 samples lost the plate-like morphology of their LDH precursors (Figure S3). The supported Ni-Ga IMC NPs on the matrix can be recognized through the TEM images in Figure 7. According to the lattice spacings, the observed NPs can be assigned to NiGa IMC ($d_{110}=0.205$ nm), Ni_5Ga_3 IMC ($d_{221}=0.209$ nm), and Ni_3Ga IMC ($d_{111}=0.207$ nm) for $NiMg_3Ga_4$ -700, $NiMg_2Ga_1$ -700, and both $Ni_5Mg_4Ga_3$ -700 and $Ni_3Mg_2Ga_1$ -700, respectively. In comparison with the $Ni_xMg_yGa_z$ -500 samples, in the $Ni_xMg_yGa_z$ -700 samples the particle size of Ni-Ga IMCs increases with the increase in the mean size from 16.9, 18.8, 17.5 to 25.8 nm. In general, IMCs obtained through conventional solid phase reactions demonstrate large particle size (> 100 nm); in contrast, Ni-Ga IMCs obtained herein possess significantly decreased particle size in spite of a high treatment temperature (700 °C) owing to the anchoring effect of the MgO matrix.^[13] In conclusion, by changing the Ni/Ga ratio in LDH precursors or reduction temperature, three types of supported Ni-Ga IMCs (NiGa, Ni_5Ga_3 , and Ni_3Ga) as well as Ni_3Ga IMCs with tunable particle size (from 4.9 to 25.8 nm) can be obtained.

Catalytic selective hydrogenation of phenylacetylene over Ni-Ga IMCs

The semihydrogenation of phenylacetylene was used as a model reaction for the evaluation of selective hydrogenation performance of these supported Ni-Ga IMC catalysts. As a reference sample, the supported Ni/MgO catalyst was synthesized by using the wet impregnation method (Figure S4). Because Ni NPs could promote the transfer hydrogenation of C-C multiple bonds by using alcohols (e.g., 2-propanol) as a H source, a control experiment in the absence of H_2 was performed over the Ni/MgO sample. No hydrogenation reaction was observed (Fig-

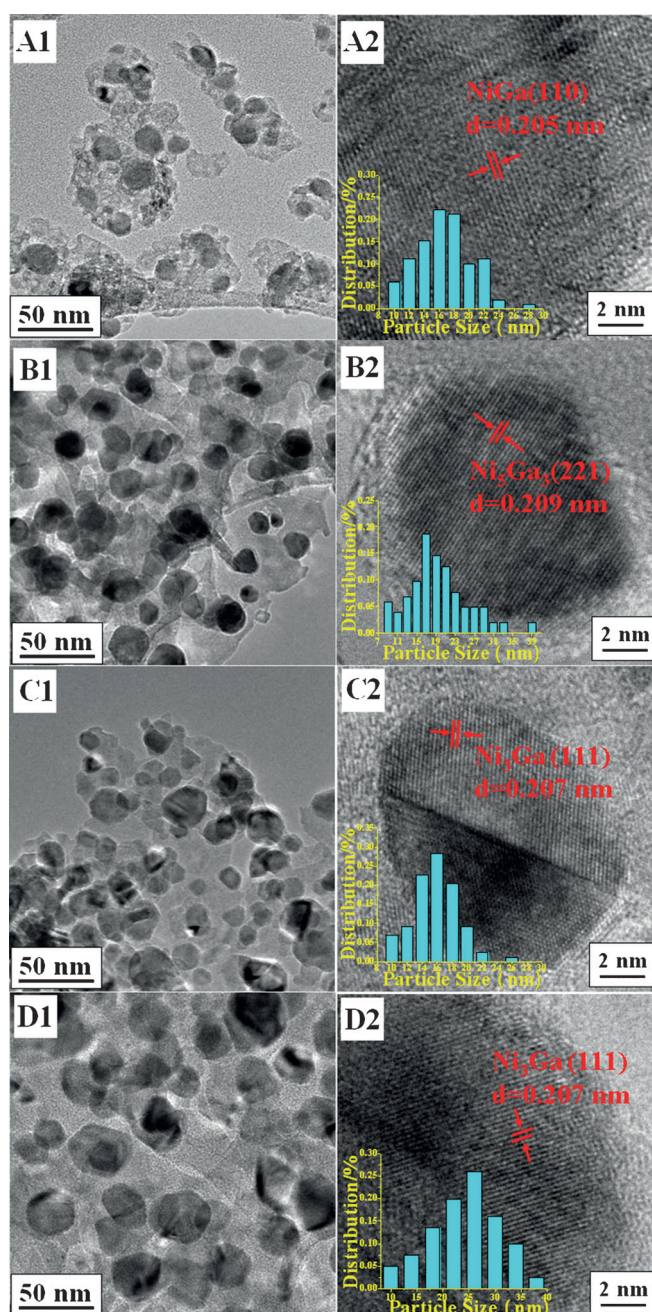


Figure 7. TEM images of the as-synthesized Ni-Ga IMCs NPs derived from the in situ reduction of $Ni_xMg_yGa_z$ LDH precursors at 700 °C: A1) $NiMg_3Ga_4$ -700, B1) $NiMg_3Ga_4$ -700, C1) $Ni_5Mg_4Ga_3$ -700, and D1) $Ni_3Mg_2Ga_1$ -700. The corresponding high-resolution TEM lattice fringe images are shown in panels A2, B2, C2, and D2, respectively. The insets show the size distribution of Ni-Ga IMC NPs with a mean value of 16.9, 18.8, 17.5, and 25.8 nm, respectively.

ure 8A and B, curve e). Thus, the $Ni_5Mg_4Ga_3$ -700 (Ni_3Ga), $NiMg_3Ga_4$ -700 (Ni_5Ga_3), and $NiMg_3Ga_4$ -700 (NiGa) samples with similar particle size are chosen to study the effect of the Ni/Ga ratio. The detailed information for these catalysts is summarized in Table S2. The catalytic conversion and the corresponding selectivity versus reaction time over Ni/MgO and $Ni_xMg_yGa_z$ -700 catalysts are plotted in Figure 8. The hydrogenation activity increases in the following order: Ni/MgO >

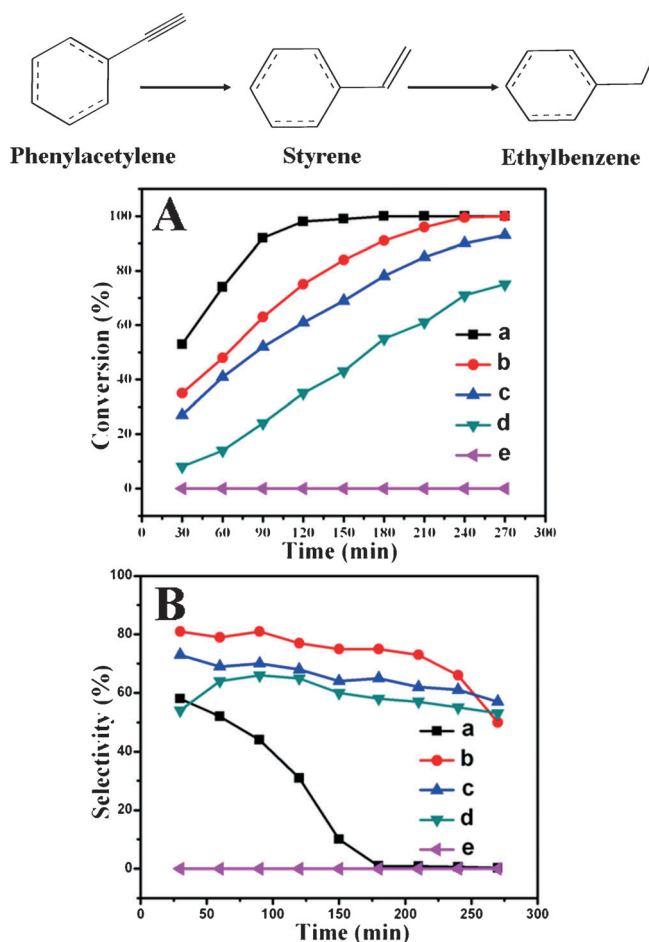


Figure 8. A) The catalytic conversion and B) the corresponding selectivity versus reaction time for the hydrogenation of phenylacetylene to styrene over different catalysts: a) Ni/MgO, b) Ni₅Mg₄Ga₃-700 (Ni₃Ga), c) NiMg₃Ga-700 (Ni₅Ga₃), d) NiMg₃Ga₄-700 (NiGa), and e) Ni/MgO tested for comparison purpose under 0.5 MPa of N₂ pressure. Reaction conditions: phenylacetylene/Ni ratio = 15; 1.0 mL of phenylacetylene; 30 mL of 2-propanol; 50 °C; 0.5 MPa of H₂ pressure (except curve e).

Ni₅Mg₄Ga₃-700 (Ni₃Ga) > NiMg₃Ga-700 (Ni₅Ga₃) > NiMg₃Ga₄-700 (NiGa). The Ni/MgO catalyst demonstrates the best hydrogenation activity but worst selectivity (Figure 8A and B, curve a), which is consistent with the previous report.^[1e,16] In contrast, the selectivity toward styrene improves dramatically over Ni–Ga IMC catalysts (Figure 8B). The Ni₅Mg₄Ga₃-700 catalyst (Ni₃Ga) with the particle size of 16.9 nm demonstrates the optimal catalytic selectivity with the styrene yield of 70.2% (conversion = 96.3% and selectivity = 72.9% at 50 °C and 0.5 MPa for 3.5 h; Figure 8B, curve b). To study the effect of the particle size of the Ni₃Ga IMC on its catalytic behavior, evaluations over Ni_xMg_yGa_z-500 samples with various particle sizes (from 4.8 to 10.9 nm) were performed (Figure S5). Notably, the catalytic activity increases with the decreased particle size and the selectivity remains the same. The styrene yield increased to 79.2% (conversion = 96.7% and selectivity = 81.9% at 50 °C and 0.5 MPa for 2.5 h) over the Ni₅Mg₄Ga₃-500 (Ni₃Ga) catalyst with the particle size of 7.2 nm. The effects of temperature and H₂ pressure on the catalytic behavior of the Ni₅Mg₄Ga₃-500 cata-

lyst (Ni₃Ga, particle size = 7.2 nm) were also studied (Figure S6). Both the increased temperature and pressure hamper the styrene selectivity. After the optimization of reaction conditions, the best catalytic performance can be obtained over the Ni₅Mg₄Ga₃-500 catalyst (Ni₃Ga, particle size = 7.2 nm) with the styrene yield of 87.7% (conversion = 95.1% and selectivity = 92.2% at 40 °C and 0.3 MPa for 5 h). For comparison purposes, we calculated the value of styrene evolution rate [mol_{styrene} h⁻¹ g_{Ni}⁻¹]. The highest styrene evolution rate was found to be 0.084 mol_{styrene} h⁻¹ m_{Ni}⁻¹ for the Ni₅Mg₄Ga₃-500 sample, which was higher than that of most of the reported Ni-based catalysts.^[1–3,16] The results demonstrate that the excellent catalytic performance of Ni–Ga IMC catalysts make them promising substitutes for noble metals for the selective hydrogenation of alkyne.

Electron and geometry structure of Ni–Ga IMCs

To gain a deep insight into the structure–function correlation, the XAFS characterization and DFT calculations were performed to elucidate the electronic structure and the atomic configuration in their local environment for the three Ni–Ga IMCs (Ni₃Ga, Ni₅Ga₃, and NiGa). The normalized Ni K-edge XANES spectra of supported Ni–Ga IMCs as well as the reference sample (Ni foil) are shown in Figure 9a. The apparent shift of the absorption edge toward low photon energy relative to the Ni foil reveals the enrichment of electrons on the Ni atom (labeled as Ni^{δ-}) in Ni–Ga IMCs.^[17] This result could be attributed to the electron transfer from the Ga atom to the Ni atom, which is in accordance with the electronegativity values of Ga (1.6) and Ni (1.9). The Fourier transform of Ni K-edge extended XAFS (EXAFS) oscillations in *R* space is shown in Figure 9b. The first nearest-neighbor distance in Ni–Ga IMCs increases to high *R* value compared with that in the Ni foil: Ni ≈ NiGa < Ni₅Ga₃ < Ni₃Ga, which indicates a strong Ni–Ga interaction in Ni–Ga IMCs through chemical bonding. The curve fitting results of these samples are listed in Table 1, which indicates that the specific Ni–Ga bond length increases from 2.50 (NiGa) to 2.52 Å (Ni₅Ga₃) and finally to 2.53 Å (Ni₃Ga). The decreased coordination number of Ni–Ga IMCs relative to that of the Ni foil (12) indicates the interspersions of Ni and Ga elements in Ni–Ga

Table 1. Curve fitting results of Ni K-edge EXAFS spectra of supported Ni₃Ga, Ni₅Ga₃, and NiGa catalysts.

Sample	Shell	CN ^[a]	<i>R</i> [Å] ^[b]	Δσ ² [Å] ^[c]
Ni foil	Ni–Ni	12	2.49	0.0012
Ni ₃ Ga	Ni–Ga	7.6 ± 1.2	2.53	0.0066
	Ga–Ni	7.4 ± 1.5	2.53	0.0051
Ni ₅ Ga ₃	Ni–Ga	6.6 ± 1.0	2.52	0.0023
	Ga–Ni	5.8 ± 0.9	2.52	0.0035
NiGa	Ga–Ni	7.5 ± 1.4	2.50	0.0011
	Ga–Ni	7.5 ± 1.4	2.50	0.0011

[a] Coordination number; [b] Distance between absorber and backscatter atoms; [c] Change in the Debye–Waller factor value relative to that of the reference sample.

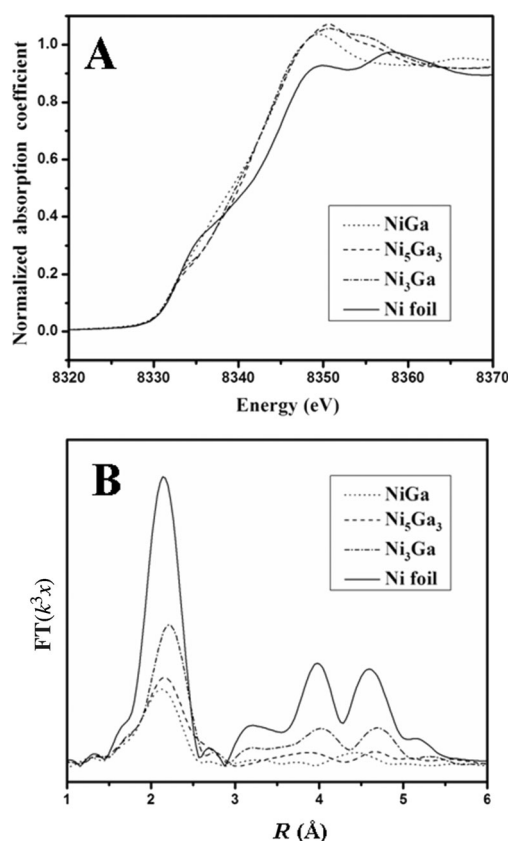


Figure 9. A) The normalized intensity of Ni K-edge XANES spectra of supported Ni–Ga IMCs and Ni foil. B) The corresponding Fourier transforms of the k^2 -weighted EXAFS spectra in R space and that of Ni foil for comparison.

IMCs, which is the unique structural feature of IMCs and is termed active-site isolation.^[4a,b]

Then, DFT calculations were performed to understand the electron and geometry structure of Ni–Ga IMCs. The structural models of Ni–Ga IMCs are shown in Figure S7, which were chosen according to the XRD patterns. The total electron density contour maps in Figure S8 demonstrate the partial overlap between Ni and Ga atoms, which indicates the strong Ni–Ga electron interaction. The electron density difference contour maps (Figure S9) demonstrate the polarization of Ni–Ga bonding, resulting from the electron transfer from the Ga atom to the Ni atom, which is consistent with the results of XAFS observations. The calculated specific charge quantity of the Ni atom increased from $-0.069e$ (Ni₃Ga) to $-0.406e$ (NiGa) with the decrease in Ni/Ga ratio in Ni–Ga IMCs.

Another unique feature of IMCs is the active-site isolation, proposed by the Schlögl group.^[4a,b] For Ni–Ga IMCs, Ni is the active component whereas Ga is inert in the catalytic hydrogenation reaction. The geometry and bonding structure in the single unit cell of Ni–Ga IMCs with the marked calculated bond length are shown in Figure 10a–c. For the face-centered cubic Ni₃Ga IMC, the Ni atom is located at the face-centered position and both Ni–Ni and Ni–Ga bonds have the same bond length (2.53 Å). The structure for Ni₅Ga₃ is much complicated, and the bond length for Ni–Ni and Ni–Ga bonds is mainly 2.52 Å at the

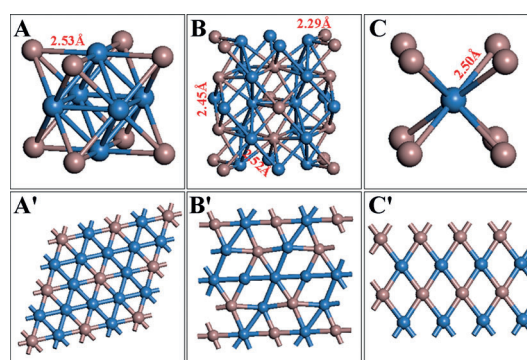


Figure 10. Result of DFT calculations for the geometry structure and the atomic bonding in a single unit cell for A) Ni₃Ga, B) Ni₅Ga₃, and C) NiGa. Their preferential crystal face for A') Ni₃Ga(111), B') Ni₅Ga₃(221), and C') NiGa(110). The partial interatomic bond length in these Ni–Ga IMCs is also labeled.

(110) face. In the case of body-centered cubic NiGa IMC, the Ni atom is located at the body-centered location and completely coordinated by the Ga atom with the same Ni–Ga bond length of 2.50 Å. The results agree well with the XAFS data in Table 1. Moreover, the site isolation of active Ni by inactive Ga in Ni–Ga IMCs can be seen in Figure 10a'–c'. With the decrease in Ni/Ga ratio, the Ni–Ni coordination decreases gradually whereas the Ni–Ga coordination increases. The Ni atom is completely separated by Ga atoms at the (110) face of the NiGa IMC.

The observed electron transfer and active-site isolation in Ni–Ga IMCs have a great effect on their catalytic performance for the selective hydrogenation of alkyne, which can be understood from the following two aspects. First, the electrons transferred from Ga to Ni occupy part vacant d-electron orbit of the Ni atom,^[18] which may decrease the adsorption capacity of the active H atom and thus inhibit the deep hydrogenation of styrene over Ni–Ga IMC catalysts. Second, it has been reported that the sequential hydrogenation of alkyne to alkene via vinyl and vinylidene intermediates requires a decreased active site size,^[4a,b] which is the same as in the Ni–Ga IMC system for the selective hydrogenation of phenylacetylene, and the significantly improved selectivity can be attributed to the charge transfer and active-site isolation in Ni–Ga IMCs. Moreover, the hydrogenation selectivity does not increase along with the improvement in electron transfer and active-site isolation in Ni–Ga IMCs. The unique structural feature of each Ni–Ga IMC, particle size, or even the support effect may also impose effects on catalytic behavior, the study of which is underway in our laboratory for further understanding.

Conclusions

We have developed a facile methodology for the preparation of supported Ni–Ga intermetallic compounds (IMCs; Ni₃Ga, Ni₅Ga₃, and NiGa) NPs with tunable size by using the layered double hydroxide (LDH) precursor method and demonstrated their excellent catalytic behavior for the selective hydrogenation of phenylacetylene. The temperature-programmed reduc-

tion by H₂ measurements reveal the Ni-promoted gradual reduction mechanism of Ga species; the particle size or type of Ni–Ga IMCs can be tuned by modulating the Ni/Ga ratio in LDH precursors or the reduction temperature during the topotactic transformation of LDHs to Ni–Ga IMCs. The resulting Ni–Ga IMCs demonstrate significantly improved catalytic selectivity for the hydrogenation of phenylacetylene to styrene, and the best catalytic activity can be obtained over the Ni₃Ga IMC with a particle size of 7.2 nm (styrene yield = 87.7% at 40 °C and 0.3 MPa), which is higher than that of most of the reported Ni catalysts. The remarkable increase in hydrogenation selectivity can be attributed to the charge transfer and active-site isolation in Ni–Ga IMCs, which is confirmed by X-ray absorption fine-structure characterization and DFT calculations. The excellent catalytic performance of Ni–Ga IMCs demonstrated herein makes them promising low-cost catalysts for the chemoselective hydrogenation of phenylacetylene.

Experimental Section

Materials

Ga(NO₃)₃·xH₂O was purchased from Sigma–Aldrich. The following analytical grade chemicals were used without further purification: NaOH, Na₂CO₃, Ni(NO₃)₂·6H₂O, and Mg(NO₃)₂·6H₂O. Deionized H₂O was used in all the experimental processes.

Synthesis of LDH precursors and supported Ni–Ga IMCs

Synthesis of Ni_xMg_yGa_z LDH precursors

Ni_xMg_yGa_z LDHs with different Ni/Mg/Ga molar ratios (labeled as NiMg₃Ga₄-LDHs, NiMg₃Ga-LDHs, Ni₂Mg₄Ga₃-LDHs, and Ni₃Mg₂Ga-LDHs) were synthesized by using a coprecipitation method. Typically, Ni(NO₃)₂·6H₂O, Mg(NO₃)₂·6H₂O, and Ga(NO₃)₃ with a given ratio of Ni²⁺/Mg²⁺/Ga³⁺ were dissolved in deionized H₂O (100 mL) to obtain a solution with a total cationic concentration (0.15 M, solution A). A certain amount of NaOH and Na₂CO₃ were dissolved together to give a base solution (100 mL, solution B, [CO₃²⁻] = 2.0 [M³⁺], [OH⁻] = 1.8([M²⁺] + [M³⁺])). Solutions A and B were then mixed together at a steady rate of 3000 rpm for 1 min. The resulting suspension was aged in a sealed Teflon autoclave at 125 °C for 24 h. All the obtained precipitate was washed thoroughly with H₂O and dried in an oven at 60 °C overnight.

Synthesis of supported Ni–Ga IMCs

Various supported Ni–Ga IMCs were obtained by using an in situ reduction process of the LDH precursors. In a typical method, LDHs (1.0 g) were reduced in a H₂/N₂ (50:50, v/v) stream at 500 or 700 °C for 5 h (initial heating rate = 2 °C min⁻¹). The reduction process results in the phase transformation from LDHs to Ni–Ga IMCs. The resulting product was slowly cooled to the reaction temperature in a N₂ stream for the subsequent catalytic evaluation.

Synthesis of Ni/MgO

The Ni/MgO sample was prepared by using the conventional impregnation method for comparison purposes. MgO (1.0 g, J&K Chemicals Ltd, ≈ 50 nm) was added in a Ni(NO₃)₂·6H₂O solution (10 mL, 0.34 M) for 24 h and then dried at 60 °C overnight. The re-

sulting sample was calcined in air at 400 °C for 4 h and then reduced by flowing H₂ at 700 °C for 5 h. The Ni content was adjusted to ≈ 20 wt %.

Catalytic evaluation for the selective hydrogenation of phenylacetylene

In a typical method, the catalyst (0.05 g), phenylacetylene (1 mL), and 2-propanol solution (30 mL) were placed into a stainless steel reaction reactor, which was fitted inside a Teflon tank. To compare these Ni-based catalysts, the total Ni content of each catalyst was maintained at the same level by changing the catalyst consumption in the catalytic test according to the inductively coupled plasma results (see Table S2). The air in the vessel was replaced thrice with H₂ with a pressure of 3.5 MPa, vented, and sealed. After the reactor temperature was increased to the target temperature (e.g., 50 °C), H₂ was introduced into the reactor with an initial pressure of 0.5 MPa. After a given reaction time, the reaction product was analyzed off-line by using GC (Shimadzu GC-2014C equipped with a flame ionization detector) or by GC–MS (Shimadzu GC-2010).

Characterization

H₂-TPR was performed in a quartz tube reactor on a Micromeritics ChemiSorb 2720 equipped with a thermal conductivity detector. In each case, the sample (100 mg) was sealed and pretreated at 200 °C in N₂ atmosphere for 2 h in the reactor and then a gaseous mixture of H₂ and Ar (1:9, v/v) was fed to the reactor at 40 mL min⁻¹. The temperature was increased to 1000 °C (heating rate = 10 °C min⁻¹). The powder XRD measurements were performed on a Rigaku XRD-6000 diffractometer using CuK_α radiation (λ = 0.15418 nm) at 40 kV, 40 mA, a scanning rate of 10 ° min⁻¹, and 2θ = 3–90°. The Ni XAFS measurements were performed with the 1W1B-XAFS beam line at the Beijing Synchrotron Radiation Facility, Institute of High Energy Physics, Chinese Academy of Sciences. The element content in the samples was determined from inductively coupled plasma atomic emission spectroscopy analysis (Shimadzu ICPS-7500). The morphology of the samples was investigated by using a Zeiss Supra 55 scanning electron microscope operating at an accelerating voltage of 20 kV in combination with energy dispersive X-ray spectroscopy for the determination of metal composition. The TEM images were recorded with JEOL JEM-2010 high-resolution transmission electron microscopes operating at an accelerating voltage of 200 kV.

Computational methods

All calculations were performed with the periodic DFT method using Dmol3 module in Material Studio 5.5 software package (Accelrys Inc., San, Diego, CA).¹⁹ The single crystal cell structural models for Ni₃Ga, Ni₅Ga₃, and NiGa were built according to the previous reports,²⁰ in which the crystal structure is consistent with our experimental results: Ni₃Ga, *Pm̄3m*(221); Ni₅Ga₃, *Cmmm*(65); NiGa, *Pm̄3m*(221) (see details in the Supporting Information). The generalized gradient approximation with the Perdew–Burke–Ernzerhof²¹ functional and effective core potentials with double-numeric quality basis were used for the geometric optimization and single-point energy calculations. For the calculations, the convergence tolerance was set as follows: energy = 1.0 × 10⁻⁶ Ha, force = 1.0 × 10⁻³ Ha Å⁻¹, and displacement = 1.0 × 10⁻³ Å.

Acknowledgements

This work was supported by the 973 Program (grant no. 2011CBA00504), the National Natural Science Foundation of China, the Scientific Fund from Beijing Municipal Commission of Education (20111001002), and the Fundamental Research Funds for the Central Universities (ZD1303). M.W. appreciates the financial aid received from the China National Funds for Distinguished Young Scientists of the National Natural Science Foundation of China.

Keywords: hydrogenation · intermetallic phases · gallium · nanoparticles · nickel

- [1] a) B. R. Maurer, M. Galobardes, US Pat. 4822936, **1989**; b) T. Vergunst, F. Kapteijn, J. A. Moulijn, *Ind. Eng. Chem. Res.* **2001**, *40*, 2801; c) Z. F. Shao, C. Li, X. Chen, M. Pang, X. K. Wang, C. H. Liang, *ChemCatChem* **2010**, *2*, 1555; d) W. Liu, C. O. Arean, S. Bordiga, E. Groppo, A. Zecchina, *ChemCatChem* **2011**, *3*, 222; e) J. Chung, C. Kim, H. Jeong, T. Yu, H. Binh, J. Jang, J. Lee, B. M. Kim, B. Lim, *Chem. Asian J.* **2013**, *8*, 919; f) M. P. Conley, R. M. Drost, M. Baffert, E. Gajan, C. Elsevier, W. T. Franks, H. Oshchkinat, L. Veyre, A. Zagdoun, A. Rossini, M. Lelli, A. Lesage, G. Casano, O. Ouari, P. Tordo, L. Emsléy, C. Coperet, C. Thieuleux, *Chem. Eur. J.* **2013**, *19*, 12234; g) Y. Yabe, Y. Sawama, T. Yamada, S. Nagata, Y. Monguchi, H. Sajiki, *ChemCatChem* **2013**, *5*, 2360; h) X. Chen, A. Q. Zhao, Z. F. Shao, Z. Q. Ma, C. H. Liang, *Stud. Surf. Sci. Catal.* **2010**, *175*, 77.
- [2] S. Domínguez-Domínguez, Á. Berenguer-Murcia, D. Cazorla-Amorós, Á. Linares-Solano, *J. Catal.* **2006**, *243*, 74.
- [3] a) S. Domínguez-Domínguez, Á. Berenguer-Murcia, B. K. Pradhan, Á. Linares-Solano, D. Cazorla-Amorós, *J. Phys. Chem. C* **2008**, *112*, 3827; b) S. Domínguez-Domínguez, Á. Berenguer-Murcia, Á. Linares-Solano, D. Cazorla-Amorós, *J. Catal.* **2008**, *257*, 87; c) P. Weerachawanasak, O. Mekasuwandumrong, M. Arai, S. I. Eujita, P. Praserttham, J. Panpranot, *J. Catal.* **2009**, *262*, 199; d) N. Tiengchad, O. Mekasuwandumrong, C. Na-Chiangmai, P. Weerachawanasak, J. Panpranot, *Catal. Commun.* **2011**, *12*, 910.
- [4] a) J. Osswald, R. Giedigkeit, R. E. Jentoft, M. Armbrüster, F. Girgsdies, K. Kovnir, T. Ressler, Yu. Grin, R. Schlögl, *J. Catal.* **2008**, *258*, 210; b) J. Osswald, K. Kovnir, M. Armbrüster, R. Giedigkeit, R. E. Jentoft, U. Wild, Yu. Grin, R. Schlögl, *J. Catal.* **2008**, *258*, 219; c) L. D. Li, B. S. Zhang, E. Kunkes, K. Föttinger, M. Armbrüster, D. S. Su, W. Wei, R. Schlögl, M. Behrens, *ChemCatChem* **2012**, *4*, 1764; d) M. Armbrüster, M. Behrens, F. Cinquini, K. Föttinger, Y. Luo, A. Haghofer, B. Klötzer, A. Knop-Geriche, H. Lorenz, A. Ota, S. Penner, J. Prinz, C. Rameshan, Z. Révay, D. Rosenthal, G. Rupprechter, P. Sautet, R. Schlögl, L. D. Shao, L. Szentmiklósi, D. Teschner, D. Torres, R. Wagner, R. Widmer, G. Wowsnick, *ChemCatChem* **2012**, *4*, 1048; e) P. P. Sun, G. Siddiqi, M. F. Chi, A. T. Bell, *J. Catal.* **2010**, *274*, 192; f) P. P. Sun, G. Siddiqi, W. C. Vining, M. F. Chi, A. T. Bell, *J. Catal.* **2011**, *282*, 165.
- [5] a) J. Ruiz-Martínez, Y. Fukui, T. Komatsu, A. Sepúlveda-Escribano, *J. Catal.* **2008**, *150*, 70; b) K. S. Rodiansono, T. Hara, N. Ichikuni, S. Shimazu, *Catal. Sci. Technol.* **2012**, *2*, 2139.
- [6] a) A. Ota, E. L. Kunkes, I. Kasatkin, E. Groppo, D. Ferri, B. Poceiro, R. M. N. Yerga, M. Behrens, *J. Catal.* **2012**, *293*, 27; b) S. E. Collins, J. J. Delgado, C. Mira, J. J. Calvino, S. Bernal, D. L. Chiavassa, M. A. Baltanás, A. L. Bonivardi, *J. Catal.* **2012**, *292*, 90.
- [7] a) H. Abe, F. Matsumoto, L. R. Alden, S. C. Warren, H. D. Abruña, F. J. Disalvo, *J. Am. Chem. Soc.* **2008**, *130*, 5452; b) E. Casado-Rivera, D. J. Volpe, L. Alden, C. Lind, C. Downie, T. Vazquez-Alvarez, A. C. D. Angelo, F. J. Disalvo, H. D. Abruña, *J. Am. Chem. Soc.* **2004**, *126*, 4043.
- [8] a) M. Armbrüster, G. Wowsnick, M. Friedrich, M. Heggen, R. Cardoso-Gil, *J. Am. Chem. Soc.* **2011**, *133*, 9112; b) M. Armbrüster, K. Kovnir, M. Behrens, D. Teschner, Yu. Grin, R. Schlögl, *J. Am. Chem. Soc.* **2010**, *132*, 14745; c) R. Leary, F. D. L. Peña, J. S. Barnard, Y. Luo, M. Armbrüster, S. J. M. Thomass, P. A. Midgley, *ChemCatChem* **2013**, *5*, 2599.
- [9] M. Armbrüster, K. Kovnir, M. Friedrich, D. Teschner, G. Wowsnick, M. Hahne, P. Gille, L. Szentmiklósi, M. Feuerbacher, M. Heggen, F. Girgsdies, D. Dosenthal, R. Schlögl, Yu. Grin, *Nat. Mater.* **2012**, *11*, 690.
- [10] a) J. W. Lekse, T. J. Stagger, J. A. Aitken, *Chem. Mater.* **2007**, *19*, 3601; b) N. H. Chou, R. E. Schaak, *J. Am. Chem. Soc.* **2007**, *129*, 7339.
- [11] a) G. R. Williams, D. O'Hare, *J. Mater. Chem.* **2006**, *16*, 3065; b) A. M. Fogg, A. L. Rohl, G. M. Parkinson, D. O'Hare, *Chem. Mater.* **1999**, *11*, 1194; c) S. He, S. T. Zhang, J. Lu, Y. F. Zhao, J. Ma, M. Wei, D. G. Evans, X. Duan, *Chem. Commun.* **2011**, *47*, 10797; d) L. Li, Y. Feng, Y. Li, W. Zhao, J. Shi, *Angew. Chem.* **2009**, *121*, 6002; *Angew. Chem. Int. Ed.* **2009**, *48*, 5888.
- [12] a) H. C. Liu, E. Z. Min, *Green Chem.* **2006**, *8*, 657; b) K. H. Goh, T. T. Lim, Z. L. Dong, *Water Res.* **2008**, *42*, 1343.
- [13] a) M. Q. Zhao, Q. Zhang, W. Zhang, G. Q. Huang, Y. H. Zhang, D. S. Su, F. Wei, *J. Am. Chem. Soc.* **2010**, *132*, 14739; b) S. He, Z. An, M. Wei, D. G. Evans, X. Duan, *Chem. Commun.* **2013**, *49*, 5912; c) S. He, C. M. Li, H. Chen, D. S. Su, B. S. Zhang, X. Z. Cao, B. Y. Wang, M. Wei, D. G. Evans, X. Duan, *Chem. Mater.* **2013**, *25*, 1040; d) C. M. Li, Y. D. Chen, S. T. Zhang, S. M. Xu, J. Y. Zhou, F. Wang, M. Wei, D. G. Evans, X. Duan, *Chem. Mater.* **2013**, DOI: 10.1021/cm4021832.
- [14] S. Collins, G. Finos, R. Alcántara, E. D. Rio, S. Bernal, A. Bonivardi, *Appl. Catal. A* **2010**, *388*, 202.
- [15] H. Okamoto, *J. Phase Equilib. Diffus.* **2008**, *29*, 296.
- [16] X. Chen, A. Zhao, Z. F. Shao, C. Li, C. T. Williams, C. H. Liang, *J. Phys. Chem. C* **2010**, *114*, 16525.
- [17] a) S. Alayoglu, P. Zavalij, B. Eichhorn, Q. Wang, A. I. Frenkel, P. Chupas, *ACS Nano* **2009**, *3*, 3127; b) A. Onda, T. Komatsu, T. Yashima, *J. Catal.* **2004**, *221*, 378.
- [18] L.-S. Hsu, A. I. Nesvizhskii, *J. Phys. Chem. Solids* **2001**, *62*, 1103.
- [19] a) M. D. Segall, P. J. D. Lindan, M. J. Probert, J. Pickard, P. J. Hasnip, S. J. Clark, M. C. Payne, *J. Phys. Condens. Matter* **2002**, *14*, 2717; b) B. Delley, *J. Chem. Phys.* **1990**, *92*, 508.
- [20] a) Y. Mishima, S. Ochiai, T. Suzuki, *Acta Metall.* **1985**, *33*, 1161; b) S. Bhan, K. Schubert, *J. Less-Common Met.* **1969**, *17*, 73; c) R. Guerin, A. Guivarc'h, *J. Appl. Phys.* **1989**, *66*, 2122.
- [21] P. J. Sideris, U. G. Nielsen, Z. Gan, C. P. Grey, *Science* **2008**, *321*, 113.

Received: September 24, 2013

Revised: December 8, 2013

Published online on February 12, 2014